

Increased structural white and grey matter network connectivity compensates for functional decline in early multiple sclerosis

Vinzenz Fleischer, Adriane Gröger, Nabin Koirala, Amgad Drobby, Muthuraman Muthuraman, Pierre Kolber, Eva Reuter, Sven G Meuth, Frauke Zipp and Sergiu Groppa

Abstract

Background: The pathology of multiple sclerosis (MS) consists of demyelination and neuronal injury, which occur early in the disease; yet, remission phases indicate repair. Whether and how the central nervous system (CNS) maintains homeostasis to counteract clinical impairment is not known.

Objective: We analyse the structural connectivity of white matter (WM) and grey matter (GM) networks to understand the absence of clinical decline as the disease progresses.

Methods: A total of 138 relapsing–remitting MS patients (classified into six groups by disease duration) and 32 healthy controls were investigated using 3-Tesla magnetic resonance imaging (MRI). Networks were analysed using graph theoretical approaches based on connectivity patterns derived from diffusion-tensor imaging with probabilistic tractography for WM and voxel-based morphometry and regional-volume-correlation matrix for GM.

Results: In the first year after disease onset, WM networks evolved to a structure of increased modularity, strengthened local connectivity and increased local clustering while no clinical decline occurred. GM networks showed a similar dynamic of increasing modularity. This modified connectivity pattern mainly involved the cerebellum, cingulum and temporo-parietal regions. Clinical impairment was associated at later disease stages with a divergence of the network patterns.

Conclusion: Our findings suggest that network functionality in MS is maintained through structural adaptation towards increased local and modular connectivity, patterns linked to adaptability and homeostasis.

Keywords: Structural network reorganization, modularity, connectivity, network dynamics, early multiple sclerosis, adaptation

Introduction

Multiple sclerosis (MS) is a chronic neuroinflammatory disease of the central nervous system (CNS) leading to progressive clinical disability. The pathophysiological mechanisms are not yet completely understood, although important hallmarks have been identified in recent years.^{1,2} The underlying pathology is characterized by inflammation and demyelination manifesting as focal lesions, as well as by ongoing neurodegeneration. Furthermore, repair processes and functional and structural reorganization occur concurrently at different disease stages. Characterization of these processes is essential to understand the disease

pathophysiology and may help to identify and exploit repair strategies.

Processes of adaptation and reorganization (e.g. tissue remodelling) cannot be monitored directly using standard magnetic resonance (MR) techniques. Conventional protocols such as T2-weighted lesion load correlate only weakly with clinical disability,^{3,4} and in addition to visible T2 lesions, normal-appearing white matter (NAWM) and grey matter (GM) tissues are diffusely but strikingly affected in MS. This leads to disruptions of the connectivity pattern and is primarily responsible for motor deficits or cognitive

Correspondence to:

S Groppa

Department of Neurology and Neuroimaging Center (NIC), Focus Program Translational Neuroscience (FTN), Rhine-Main Neuroscience Network (rmn²), University Medical Center of the Johannes Gutenberg University Mainz, Langenbeckstr. 1, 55131 Mainz, Germany.
segroppa@uni-mainz.de

Vinzenz Fleischer
Adriane Gröger
Nabin Koirala
Amgad Drobby
Muthuraman Muthuraman
Pierre Kolber
Eva Reuter
Frauke Zipp
Sergiu Groppa
Department of Neurology and Neuroimaging Center (NIC), Focus Program Translational Neuroscience (FTN), Rhine-Main Neuroscience Network (rmn²), University Medical Center of the Johannes Gutenberg University Mainz, Mainz, Germany

Sven G Meuth
Department of Neurology, University of Münster, Münster, Germany

Table 1. Demographic data and MRI volume measurements of all patients.

Demographics	RRMS patients ($n=138$)
Gender (male/female)	45/93
Mean age (SD), years	33.9 (10.3)
Mean age at diagnosis (SD), years	31.2 (10.2)
Mean disease duration (SD), months	26.0 (26.0)
Median EDSS, range	1.3 (0–4)
Volumetric analysis	
Mean WM volume (SD), mL	561.1 (77.3)
Mean GM volume (SD), mL	625.8 (68.8)
Mean TB volume (SD), mL	1417.2 (141.8)
Mean T2 lesion volume (SD), mL	6.2 (9.7)

RRMS: relapsing-remitting multiple sclerosis; SD: standard deviation; EDSS: expanded disability status scale; WM: white matter; GM: grey matter; TB: total brain.

decline.⁵ Adaptive processes of plasticity occur in the extended GM and WM networks rather at the focal lesion sites.^{6,7} Therefore, it is imperative to consider the entire brain network.

Network topology properties defined within graph theoretical analyses have become important measurable characteristics that explain healthy brain dynamics and could precisely model brain disorders.^{8,9} Specific topology patterns have been linked to adaptability and may be closely related to the clinical performance.^{8,10}

In this study, three hypotheses were tested. The first is that the structural network connectome in MS patients derived from different modalities can identify characteristic connectivity patterns in different stages of the disease. The second hypothesis is that damage to WM (involving diffuse inflammation and local demyelination) and GM (involving cortical demyelination and neuro-axonal loss) occurs simultaneously in MS.¹¹ Finally, we hypothesized that the changes in network connectivity reflect the clinical performance of relapsing-remitting multiple sclerosis (RRMS) patients.

Materials and methods

Patients

Patients were recruited at the Department of Neurology of the Johannes Gutenberg University of Mainz and measured with a standardized magnetic resonance imaging (MRI) protocol.¹² Informed consent was obtained from subjects in this study, which was approved by the local ethics committee. All patients fulfilled the revised McDonald diagnostic criteria¹³ and were assessed by an experienced neurologist, and the Expanded Disability Status Scale (EDSS) score was determined.

In this study, we included 138 patients (mean age 33.9 years; standard deviation (SD) 10.3 years) with RRMS. Demographic data are presented in Table 1.

Six groups of different disease durations were constructed: 0–6 months ($n=33$), 6–12 months ($n=17$), 12–18 months ($n=20$), 18–24 months ($n=18$), 24–48 months ($n=22$) and 48–96 months ($n=28$). The first four groups were defined to closely reflect early effects (first 2 years of the disease) and the latter two to address longer-term network properties.

We also enrolled a group of 32 age-matched healthy controls (mean age 31.8 years; SD 9.2 years) and compared them with the first group of newly diagnosed patients (0–6 months) to assess the initial direction of the changes in network connectivity.

Data acquisition

MRI was performed on a 3-Tesla scanner (Magnetom Tim Trio; Siemens) with a 32-channel receive-only head coil at the Neuroimaging Centre (NIC) Mainz, Germany. A detailed description of all sequences used for this study is given in the supplement.

Diffusion tensor imaging preprocessing

Image data were processed using FSL 5.0.8. A detailed protocol can be found elsewhere.^{14,15} Here, we give only a brief description of the aspects relevant to the study. For eddy current correction and further analysis, we used the diffusion toolbox (FDT, part of FSL) and calculated the quantitative measures of fractional anisotropy. The crossing-fibre distribution was estimated using BEDPOSTX (implemented in FSL), and the probabilities of major (f_1) and secondary (f_2)

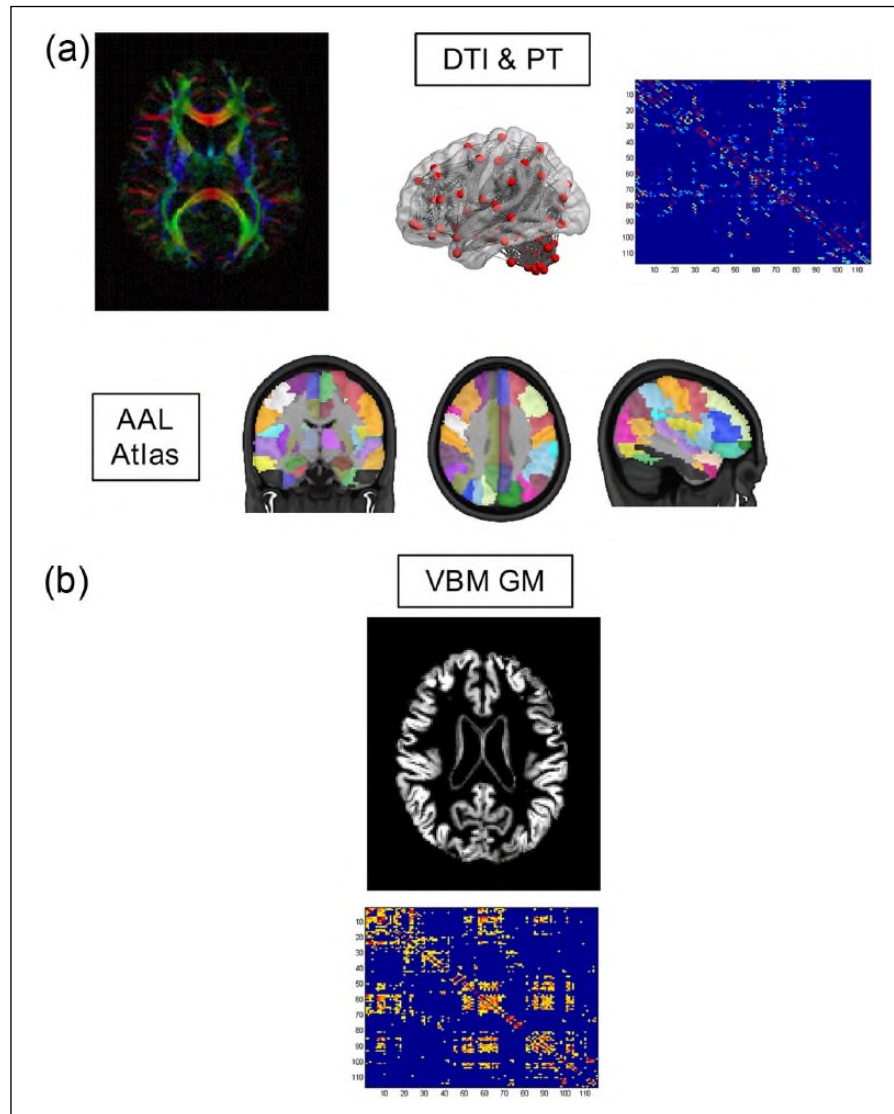


Figure 1. Study design: (a) structural connectivity matrices derived from individual DTI and probabilistic tractography analysis and (b) group analysis of grey matter. In the middle is a scheme of the AAL atlas for nodes' definition in the connectivity analysis.

fibre directions were calculated.¹⁶ All images were aligned and affine-transformed into the standard stereotactic space MNI-152.

Probabilistic tractography and network reconstruction

For probabilistic tractography (PT), we built seed masks for 116 regions defined by the Automated Anatomical Labelling (AAL) atlas.¹⁷ The aim of our tractography analysis was to generate region of interest (ROI)-based connectivity index maps for the entire diffusion network. A multi-fibre model was fitted to the diffusion data at each voxel, allowing fibres

to be traced through regions of crossing or complexity.¹⁸ The PT connectivity matrices PT_{ij} (size 116×116) were generated for each subject and normalized on the individual level by dividing, voxel-wise, the number of streamlines passing through the voxel by the total number of the obtained streamlines. These connectivity matrices were further included in the network analysis (Figure 1).

Voxel-based morphometry preprocessing and network reconstruction

For the voxel-based morphometry (VBM) analysis, the statistical parameter mapping (SPM8) software

(<http://www.fil.ion.ucl.ac.uk/spm>) with Lesion Segmentation Tool (LST) and VBM8 toolboxes were used.¹⁹ Detailed information about the lesion-filling method is given in the supplement. For GM network reconstruction, we applied the same node definition as above. For each ROI of the AAL atlas, we extracted the individual GM value using the REX toolbox. The extracted regional intensity data were used to construct the structural correlation matrices S_{ij} for each group. In the S_{ij} (size 116×116) matrices, each element represented Pearson's correlation coefficient between ROI values across subjects in one group (Figure 1).

Network analysis

For the PT_{ij} -connectivity matrices, we calculated network measures at the single-subject level. For the VBM GM- S_{ij} -connectivity matrices, we calculated network measures for each group. Then, the network topological properties were derived from connectivity matrices at the single-subject level for WM and group level for GM. As the main aim of our study was the integrative analysis of WM and GM, we applied optimized and validated algorithms for each compartment.^{20–22}

In a last step, we performed a community structure analysis of the significant diffusion tensor imaging (DTI) and VBM GM networks for the number and anatomical distribution of the involved regions. We juxtaposed newly diagnosed patients (0–6 months) with patients with the longest disease duration (48–96 months) to consider the complete range of the studied groups.

The normalized connectivity matrices were analysed within the graph theoretical framework using the BCT toolbox.²³ We concentrated on the following measures of network topology.

Modularity was defined as the relationship between intra- and inter-module connections and describes a benefit function measuring the quality of a division of a network into communities. The *clustering coefficient* was calculated to reflect the number of connections between the neighbour's nodes and is a parameter associated with the robustness of a network. *Local efficiency* has been introduced to describe local integration as the average of the inverse distance in the network. Finally, *global efficiency* is a network integration parameter to describe information flow over the entire network. For detailed description, references and formula, please see the supplemental data.

Statistical analysis

Statistical analysis was performed using SPSS (Chicago, IL, USA). A one-way analysis of variance (ANOVA) was performed to assess differences in the clinical and volumetric parameters between the groups. Besides comparing lesion volumes between the groups, we also performed a non-parametric permutation inference using the 'randomize' function in the FSL toolbox between the groups in order to determine potential differences in the spatial distribution of the lesions.

For the individual network topological measurements derived from DTI and PT (for WM network reconstruction), a one-way ANOVA was calculated. In cases of a significant F value, we performed post hoc pairwise comparisons with least significant differences (LSD) ($p < 0.05$; two-tailed).

For the group network topological measurements derived from VBM (for GM network reconstruction), a linear regression analysis was used to examine the tendency of the network parameters (modularity, clustering coefficient, local and global efficiency) to change with disease duration and T2 WM lesion volume, each separately.

Results

Clinical data and morphometric analysis

To identify connectivity patterns in different stages of the disease, we classified patients according to disease duration, ($F(5, 137) = 1.15, p < 0.001$) (Figure 2 and Table 2). EDSS differed between groups ($F(5, 137) = 2.31, p < 0.05$); post hoc comparisons revealed differences between patients with a disease duration longer than 4 years (48–96 months) in comparison with other groups (vs 6–12 months ($p = 0.049$), vs 12–18 months ($p = 0.002$) or vs 18–24 months ($p = 0.050$), Figure 2). The measurements of the volumetric characteristics did not differ between the six groups. In particular, there were no differences in lesion volumes ($F(5, 137) = 1.70, p > 0.05$) (see Table 2) and the lesion mapping analysis revealed no differences between the six groups in lesion localization ($p > 0.05$, clusters corrected).

WM network reorganization

The graph theoretical analysis of the PT connectivity data revealed a significant modification of the WM networks at early disease stages. In the first year after disease onset, modularity increases clearly ($F(5, 137) = 2.562, p < 0.05$). Post hoc tests revealed

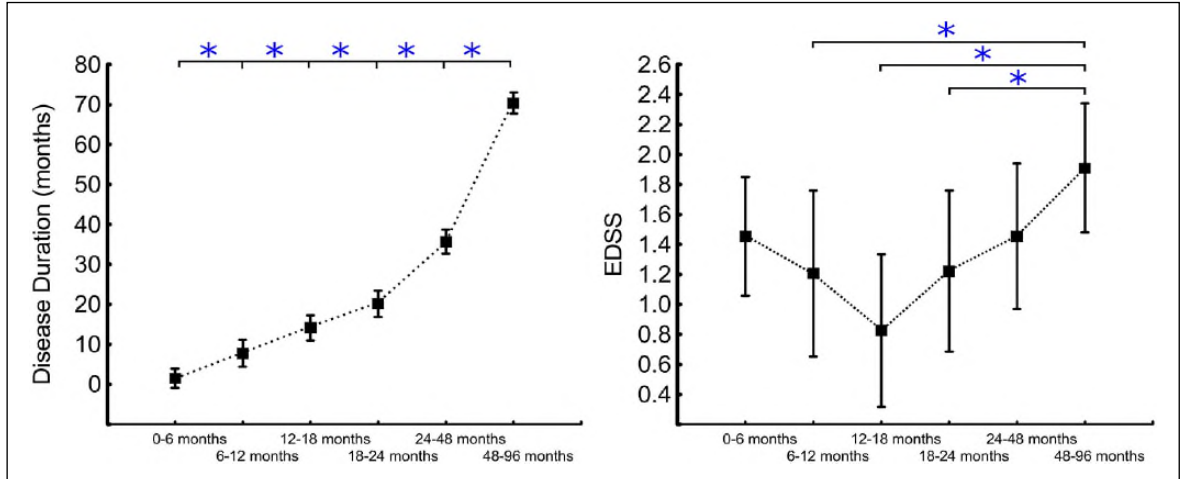


Figure 2. Clinical data. Left panel: Disease duration between the six groups. Right panel: EDSS between the six groups. * $p < 0.05$.

Table 2. Demographic data and MRI volume measurements separated into six groups based on the RRMS patients' disease duration.

	Disease duration						<i>p</i> value
	0–6 months (<i>n</i> =33)	6–12 months (<i>n</i> =17)	12–18 months (<i>n</i> =20)	18–24 months (<i>n</i> =18)	24–48 months (<i>n</i> =22)	48–96 months (<i>n</i> =28)	
Demographics							
Gender (male/female)	6/27	6/11	8/12	5/13	7/15	13/15	n.s. ^a
Mean age (SD), years	32.7 (10.3)	36.9 (14.9)	31.2 (8.7)	34.8 (6.5)	32.0 (9.6)	36.3 (10.1)	n.s. ^b
Mean age at diagnosis (SD), years	32.5 (10.4)	26.2 (15.0)	30.1 (8.7)	33.1 (6.4)	29.1 (9.6)	30.3 (9.8)	n.s. ^b
Mean disease duration (SD), months	1.5 (1.7)	7.8 (1.6)	14.1 (1.4)	20.2 (1.6)	35.7 (6.4)	70.4 (14.3)	0.000 ^{b,c}
Median EDSS, range	1.5 (0–3.5)	1.0 (0–4)	0.5 (0–3)	1.3 (0–3)	1.3 (0–4)	1.8 (0–3.5)	0.048 ^{b,d}
Volumetric analysis							
Mean WM volume (SD), mL	561.2 (73.9)	563.8 (76.5)	566.3 (97.6)	545.2 (76.8)	567.6 (72.8)	560.9 (75.1)	n.s. ^b
Mean GM volume (SD), mL	630.7 (60.0)	615.7 (77.2)	621.8 (68.9)	621.3 (64.6)	634.5 (68.1)	624.9 (80.4)	n.s. ^b
Mean TB volume (SD), mL	1406.3 (129.1)	1395.7 (149.6)	1420.9 (158.5)	1398.8 (148.7)	1432.1 (117.4)	1440.7 (159.2)	n.s. ^b
Mean T2 lesion volume (SD), mL	5.4 (8.5)	4.0 (7.5)	4.2 (4.1)	3.8 (6.2)	7.6 (10.8)	10.2 (14.3)	n.s. ^b

SD: standard deviation; EDSS: expanded disability status scale; WM: white matter; GM: grey matter; TB: total brain; ANOVA: analysis of variance; LSD: least significance difference; RRMS: relapsing–remitting multiple sclerosis. Bold indicates values are statistically significant.

^aChi-square test, *p* values derived from Pearson's chi-square.

^bOne-way ANOVA, *p* values derived from between-group comparison.

^cGroup allocation was based on this variable: all post hoc comparisons with Fisher's LSD differed significantly ($p < 0.05$).

^dPost hoc comparison with LSD: $p = 0.049$ for group: 6–12 months vs group: 48–96 months and $p = 0.002$ for group: 12–18 months vs group: 48–96 months and $p = 0.050$ for group: 18–24 months vs group: 48–96 months.

significant differences between the group of newly diagnosed patients (0–6 months) and the groups with a disease duration of 12–18 months ($p = 0.005$), 18–24 months ($p = 0.012$) and 24–48 months ($p = 0.009$) (Figure 3). This increase in modularity suggests brain network reorganization towards a structure with stronger intra-module connectivity, while the

number of inter-module paths decreases. The analysis of the community structure in the WM (Figure 4) showed that the brains of patients with newly diagnosed MS had fewer connected modules ($n = 10$), while in patients with the longest disease duration the number of modules increased to 15. Furthermore, the number of regions in the modules decreased

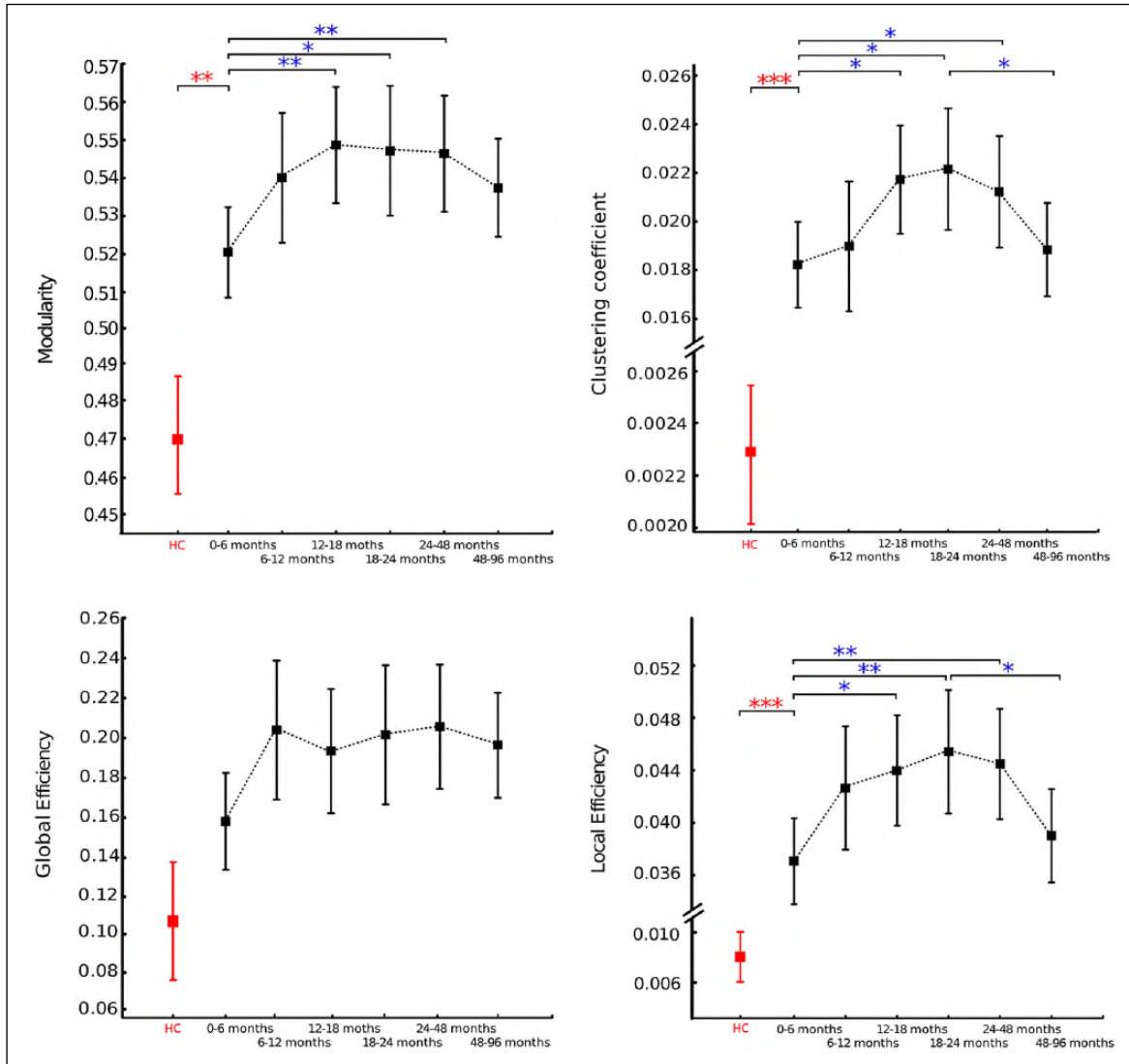


Figure 3. Network analysis. White matter network analysis showing modularity, clustering coefficient, global efficiency and local efficiency between the six groups and healthy controls. * $p < 0.05$; ** $p < 0.001$; *** $p < 0.0001$.

(Figure 4). The new modules detected in the last group (48–96 months) were located in the cerebellum, olfactory system and parieto-occipital region.

Within the first year, further local network properties evolved towards a structure with increased connectivity between neighbouring nodes. The local reorganization was reflected by an increase in clustering coefficient ($F(5, 137) = 2.466, p < 0.05$). The number of highly interconnected neighbouring nodes that form a cluster increased (significant between the group of patients with a disease duration of 0–6 months vs those with 12–18 months ($p = 0.016$), 18–24 months ($p = 0.012$) and 24–28 months ($p = 0.042$)). In the later disease stages,

however, the clustering coefficient in the group of patients with the longest disease duration decreases (18–24 months vs 48–96 months: $p = 0.04$; Figure 3).

In the early period of the disease, not only the local connectivity pattern changed but also the network capacity for local information flow increased. This was demonstrated through the significant increase in local network efficiency ($F(5, 137) = 3.058, p < 0.05$). A more strongly interconnected network with shorter path distances was observed in the group of patients with newly diagnosed MS (0–6 months) compared to the other groups (12–18 months, $p = 0.011$; 18–24 months, $p = 0.005$; 24–48 months, $p = 0.007$). Analogously to the clustering coefficient, a decrease

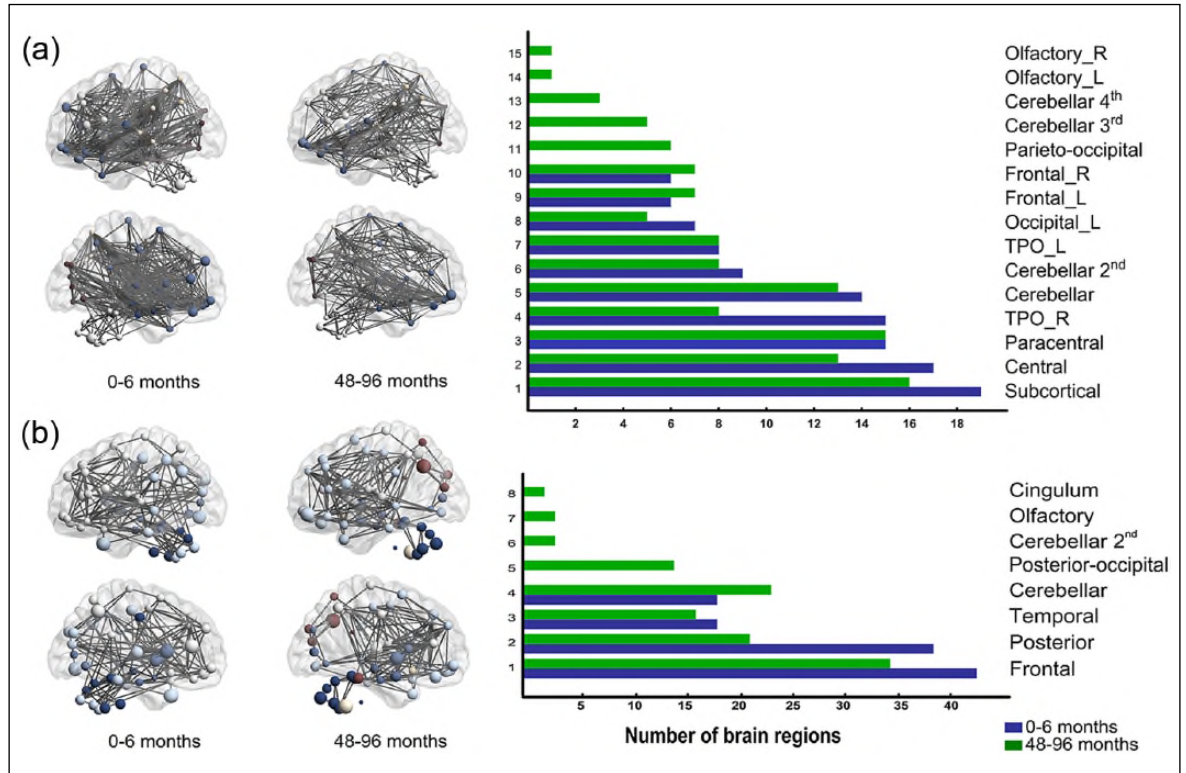


Figure 4. Left panel: Topological representation brain network and modularity data (group of newly diagnosed patients (0–6 months) and patients with the longest disease duration (48–96 months) as derived from (a) DTI and probabilistic tractography and (b) grey matter VBM. The size and colour of the nodes represent the clustering coefficient and module affiliation, respectively. Right panel: Histograms of the number of nodes in modules.

in local efficiency was seen in patients with the longest disease duration in comparison with the group with a disease duration of 18–24 months ($p=0.04$, Figure 3). The global efficiency did not differ between the groups ($F(5, 137)=1.81$, n.s.), showing that the overall network integrity is maintained despite local connectivity changes.

We additionally found significantly higher values for modularity ($t=-2.80$, $p=0.007$), clustering coefficient ($t=-17.48$, $p<0.001$) and local efficiency ($t=-11.6$, $p<0.001$) in the group of newly diagnosed patients (0–6 months) compared to controls. Global efficiency did not differ between controls and newly diagnosed patients ($t=-1.48$, $p=0.14$).

GM network reorganization

Our VBM GM network analysis showed a linear correlation of the topological network properties with two clinical parameters, namely, disease duration and T2 WM lesion volume. Modularity increases with disease duration ($r=0.85$, $p<0.05$), reflecting an increased intra-modular connectivity and long-range separation.

In addition, a direct linear relationship between increasing modular structure and T2 WM lesion volume was observed ($r=0.86$, $p<0.05$). In fact, only modularity derived from VBM GM (and none of the other three network parameters) correlated with disease duration and T2 WM lesion volume.

Similarly to the WM network analysis, we also compared GM network patterns of newly diagnosed patients (0–6 months) with the network parameters of controls and found higher values for modularity (0.238 vs 0.309), clustering coefficient (0.623 vs 0.637), local efficiency (0.792 vs 0.815) and also for global efficiency (0.573 vs 0.585) in the newly diagnosed patients.

In the analysis of GM architecture, we found an increase in the number of modules from 4 (group: 0–6 months) to 10 modules (group: 48–96 months; Figure 4). While the absolute number of modules increases, the number of regions within modules significantly decreases (Figure 4). Thus, as seen in the WM community analysis, the GM networks evolve to a structure of increased local processing, but further

long-range segregation. The changes to the modular GM architecture with impaired connectivity were noted in the cerebellum, cingulum and parieto-occipital region, also similarly to WM (Figure 4).

Discussion

In this study, we evaluate the reorganization of structural networks as described through a topological analysis of WM and GM connectivity. We show that both WM and GM networks present an increase in local connectivity at early disease stages and a breakdown of long-range paths. Moreover, the described connectivity changes were already seen in patients at the clinical onset in comparison with healthy controls. The WM structural reorganization thus appears to begin at disease onset and progress in the following disease stages before reaching a plateau after 1 year. GM networks exhibit a similar reorganization towards strengthened local connectivity and inter-modular segregation, but this pattern continues beyond the first year. While concurrent increases in WM and GM modularity occurred, no clinical impairment was noted. However, as WM and GM network architectures diverged in the groups of patients at later disease stages, functional impairment was apparent. In these groups, an impaired adaptability or a breakdown of homeostatic processes of structural brain networks occurs. As a clear direct relationship between modularity and adaptability of brain networks has been recently made,^{24,25} we postulate that the observed processes of network reorganization are putative mechanisms to compensate for ongoing diffuse damage and are essential to maintain network functioning.

WM network reorganization

In the first year of MS, WM networks evolve to a topology of increased modularity. Since modularity mirrors the relationship between intra- and inter-module connections, the described increase might be explained by a strengthening of local connections and a decrease in long-range effectiveness. Several studies have presented evidence that community structure properties of the brain and especially modularity increases can be linked to maintenance of function despite ageing or continuous damage, as shown in neurodegenerative disorders.^{25,26} Together, this emphasizes that the observed network architecture changes are not only a consequence of diffuse tissue damage but should be seen as integral processes for optimal network functioning.

A notable increase in the modular structure of functional networks has been recently demonstrated in

early MS using functional MRI.²⁷ Although ‘early’ was defined in terms of minimal functional impairment (low EDSS), we see clear parallels between the functional reorganization as demonstrated by Gamboa et al. and that of the structural networks as shown by our data.

Moreover, increased local efficiency and clustering was noted. This means an increase in effectiveness of local information transfer. Higher clustering coefficients imply that the nearest neighbours of a node are more likely to be connected in order to maintain local information flow.

GM network reorganization

Various quantitative MR studies have indicated GM integrity changes in MS.^{28–30} Mostly atrophy, but also compensatory increases in GM fraction were reported and were more closely related to functional disability than WM changes.^{31,32} The regional pattern varied among subjects and showed different inter-individual temporal vectors.³³ All this makes the precise quantification of the GM pathology challenging. Our analysis of network topology may provide a more accurate characterization of the entire GM network and quantification of ongoing compensatory processes.

In the absence of volumetric changes, we demonstrate a reorganization of the GM networks towards an increased modular structure. This is a pattern of network architecture with locally denser connections between similar structurally and functionally interacting parts. On the microscopic level, these GM changes might take place at the columnar level. These structures with strong intra- and inter-columnar connections are the building blocks of the nodes and could contribute to the described modularity increase.³⁴ On the other hand, the reported increase in modularity speaks for long-range GM column disconnection. The entire network becomes more heterogeneous and distant areas show less microstructural uniformity.

Clinical relevance of network reorganization

Notably, our entire patient collective showed only very mild clinical impairment. Despite the significant effect seen in the ‘all group comparison’, the studied patients in the first 4 years after disease onset did not differ in EDSS. Is it then possible that the described structural reorganization compensates partially for tissue damage so that no functional decline occurs? No changes in EDSS were observed as network topology markers increased in the first year before reaching a plateau phase later on. However, we see a clinical

worsening in the group with the longest disease duration and a complementary decrease in WM network topology parameters. In our cross-sectional design, EDSS follows a U-shaped curve, whereas modularity, clustering coefficient and local efficiency follow an inverted U-shaped curve. This observation may hint towards the functional meaning of the structural network changes. Increased modularity and a better ability to transmit information at the local level might contribute to the maintenance of functional stability in the first years, while in later stages the compensatory mechanisms fail. In fact, we see a reduction in the modular structure in the group with the longest disease duration, as seen in maturation or healthy ageing.⁹

Several functional brain regions (cerebellum, cingulum, parieto-temporal cortex) were more strongly involved in the described structural network reorganization. Knowing the role of these structures for adaptive compensation,³⁵ our data highlight the relevance of these regions for maintenance of motor functions. The changes of the modular structure in the cingulum and parieto-occipital cortex might be understood in terms of their roles in cognitive and integrative processes. These structures play an essential role in attention, visual and spatial integration and working memory.

Conclusion

We conclude that the brain connectivity of MS patients reconstructed using PT for WM connections and VBM for GM connections reflects a structural reorganization occurring in response to disease pathology. The connectivity profile in both compartments indicates increased modular decomposition and local processing in early disease stages. This reorganization might be a primordial response of the brain to changing structural conditions resulting from disseminated damage in order to maintain its homeostasis. These increasing network properties become less prominent as the disease progresses further, which is accompanied by an increase in physical disability.

Acknowledgements

F.Z. and S.G. contributed equally to this work.

Declaration of Conflicting Interests

The author(s) declared no potential conflicts of interest with respect to the research, authorship, and/or publication of this article.

Funding

The author(s) disclosed receipt of the following financial support for the research, authorship, and/or

publication of this article: This work was supported by a grant from the German Research Council (DFG; CRC-TR-128 to FZ) and also received support from the Federal Ministry for Education and Research (BMBF) concerning protocol analysis and, in part, the patient cohort (KKNMS, project B7.3 to FZ).

References

1. Zipp F, Gold R and Wiendl H. Identification of inflammatory neuronal injury and prevention of neuronal damage in multiple sclerosis: Hope for novel therapies? *JAMA Neurol* 2013; 70: 1569–1574.
2. Lucchinetti CF, Popescu BF, Bunyan RF, et al. Inflammatory cortical demyelination in early multiple sclerosis. *N Engl J Med* 2011; 365: 2188–2197.
3. Geurts JJ, Reuling IE, Vrenken H, et al. MR spectroscopic evidence for thalamic and hippocampal, but not cortical, damage in multiple sclerosis. *Magn Reson Med* 2006; 55: 478–483.
4. Wuerfel J, Tysiak E, Prozorovski T, et al. Mouse model mimics multiple sclerosis in the clinico-radiological paradox. *Eur J Neurosci* 2007; 26: 190–198.
5. Hawellek DJ, Hipp JF, Lewis CM, et al. Increased functional connectivity indicates the severity of cognitive impairment in multiple sclerosis. *Proc Natl Acad Sci U S A* 2011; 108: 19066–19071.
6. Rovaris M, Judica E, Gallo A, et al. Grey matter damage predicts the evolution of primary progressive multiple sclerosis at 5 years. *Brain* 2006; 129: 2628–2634.
7. Roosendaal SD, Geurts JJ, Vrenken H, et al. Regional DTI differences in multiple sclerosis patients. *Neuroimage* 2009; 44: 1397–1403.
8. Bassett DS, Wymbs NF, Porter MA, et al. Dynamic reconfiguration of human brain networks during learning. *Proc Natl Acad Sci U S A* 2011; 108: 7641–7646.
9. Hagmann P, Sporns O, Madan N, et al. White matter maturation reshapes structural connectivity in the late developing human brain. *Proc Natl Acad Sci U S A* 2010; 107: 19067–19072.
10. Newman MEJ. Modularity and community structure in networks. *Proc Natl Acad Sci U S A* 2006; 103: 8577–8582.
11. Calabrese M, Magliozzi R, Ciccarelli O, et al. Exploring the origins of grey matter damage in multiple sclerosis. *Nat Rev Neurosci* 2015; 16: 147–158.
12. Droy A, Lukas C, Schanzer A, et al. A human post-mortem brain model for the standardization of multi-centre MRI studies. *Neuroimage* 2015; 110: 11–21.

13. Polman CH, Reingold SC, Banwell B, et al. Diagnostic criteria for multiple sclerosis: 2010 revisions to the McDonald criteria. *Ann Neurol* 2011; 69: 292–302.
14. Smith SM, Jenkinson M, Johansen-Berg H, et al. Tract-based spatial statistics: Voxelwise analysis of multi-subject diffusion data. *Neuroimage* 2006; 31: 1487–1505.
15. Groppa S, Herzog J, Falk D, et al. Physiological and anatomical decomposition of subthalamic neurostimulation effects in essential tremor. *Brain* 2014; 137: 109–121.
16. Groppa S, Muthuraman M, Otto B, et al. Subcortical substrates of TMS induced modulation of the cortico-cortical connectivity. *Brain Stimul* 2013; 6: 138–146.
17. Tzourio-Mazoyer N, Landeau B, Papathanassiou D, et al. Automated anatomical labeling of activations in SPM using a macroscopic anatomical parcellation of the MNI MRI single-subject brain. *Neuroimage* 2002; 15: 273–289.
18. Behrens TE, Woolrich MW, Jenkinson M, et al. Characterization and propagation of uncertainty in diffusion-weighted MR imaging. *Magn Reson Med* 2003; 50: 1077–1088.
19. Schmidt P, Gaser C, Arsic M, et al. An automated tool for detection of FLAIR-hyperintense white-matter lesions in Multiple Sclerosis. *Neuroimage* 2012; 59: 3774–3783.
20. Assaf Y and Pasternak O. Diffusion tensor imaging (DTI)-based white matter mapping in brain research: A review. *J Mol Neurosci* 2008; 34: 51–61.
21. Filippi M, Rocca MA, De Stefano N, et al. Magnetic resonance techniques in multiple sclerosis: The present and the future. *Arch Neurol* 2011; 68: 1514–1520.
22. Whitwell JL. Voxel-based morphometry: An automated technique for assessing structural changes in the brain. *J Neurosci* 2009; 29: 9661–9664.
23. Rubinov M and Sporns O. Complex network measures of brain connectivity: Uses and interpretations. *Neuroimage* 2010; 52: 1059–1069.
24. Kashtan N and Alon U. Spontaneous evolution of modularity and network motifs. *Proc Natl Acad Sci U S A* 2005; 102: 13773–13778.
25. Meunier D, Lambiotte R and Bullmore ET. Modular and hierarchically modular organization of brain networks. *Front Neurosci* 2010; 4: 200.
26. Meunier D, Fonlupt P, Saive A-L, et al. Modular structure of functional networks in olfactory memory. *Neuroimage* 2014; 95: 264–275.
27. Gamboa OL, Tagliazucchi E, von Wegner F, et al. Working memory performance of early MS patients correlates inversely with modularity increases in resting state functional connectivity networks. *Neuroimage* 2014; 94: 385–395.
28. De Stefano N, Matthews PM, Filippi M, et al. Evidence of early cortical atrophy in MS: Relevance to white matter changes and disability. *Neurology* 2003; 60: 1157–1162.
29. Dalton CM, Chard DT, Davies GR, et al. Early development of multiple sclerosis is associated with progressive grey matter atrophy in patients presenting with clinically isolated syndromes. *Brain* 2004; 127: 1101–1107.
30. Calabrese M, Atzori M, Bernardi V, et al. Cortical atrophy is relevant in multiple sclerosis at clinical onset. *J Neurol* 2007; 254: 1212–1220.
31. Fisher E, Lee JC, Nakamura K, et al. Gray matter atrophy in multiple sclerosis: A longitudinal study. *Ann Neurol* 2008; 64: 255–265.
32. Sanfilippo MP, Benedict RH, Weinstock-Guttman B, et al. Gray and white matter brain atrophy and neuropsychological impairment in multiple sclerosis. *Neurology* 2006; 66: 685–692.
33. Simon JH. Brain atrophy in multiple sclerosis: What we know and would like to know. *Mult Scler* 2006; 12: 679–687.
34. Douglas RJ and Martin KA. Mapping the matrix: The ways of neocortex. *Neuron* 2007; 56: 226–238.
35. Weier K, Banwell B, Cerasa A, et al. The role of the cerebellum in multiple sclerosis. *Cerebellum* 2015; 14: 364–374.